Available online at www.sciencedirect.com
SCIENCE DIRECT®
Journal of Magnetic Resonance 172 (2005) 118–132
JMR Journal of Magnetic Resonance
www.elsevier.com/locate/jmr

Residual dipolar couplings and some specific models for motional averaging☆

Michaël Deschamps*, Iain D. Campbell, Jonathan Boyd

Department of Biochemistry, Oxford University, South Parks Road, OX1 3QU Oxford, UK

Received 2 July 2004; revised 16 September 2004
Available online 11 November 2004

Abstract

The measurement of residual dipolar couplings (RDCs) from partially oriented molecules is now widely used to provide restraints for NMR structure determination. Bond vibrations, random angular fluctuations around bond vectors and conformational exchange all influence the magnitude of the experimental RDCs. The effect that angular fluctuations have upon the magnitude of RDCs is quantitatively compared using three new models (elliptic, uni-dimensional, and equally populated two site jump) and three established models (static, isotropic motion in a cone and free diffusion about a fixed symmetry axis: Woessner's model) for motional averaging in the limit that the amplitude of motion $\beta_{max} \leqslant 15$–$20°$. The influence of the different motional models on the value of R^{obs} determined from the distribution of RDCs is explored. The consequences of the different types of angular motion for the accurate determination of bond vector orientation, with respect to the alignment tensor, **A**, is investigated. The extent to which motion influences the magnitude of RDCs is compared to some non-dynamic factors affecting RDC size.

PACS: 76.60.−k
Keywords: NMR; Residual dipolar coupling; Motional averaging

1. Introduction

Residual dipolar couplings (RDCs) [1–8] from proteins dissolved in solutions containing an aligned medium such as bicelles [8], phages [9], or polyacrylamide gels [10], provide information on the orientation of individual inter-nuclear vectors, with respect to a global molecular alignment tensor, **A**. RDC datasets have proven to be especially useful and are now widely employed to provide restraints in the NMR determination of protein structure [11]. In addition, site specific dynamics provides valuable information about the flexibility of single or multi domain proteins. NMR relaxation studies [12] are most often used to characterise local dynamics in proteins. Recently two different approaches have been proposed to determine site specific order parameters that characterise the amplitude of intra-molecular dynamics of individual bond vectors using RDCs from partially aligned proteins [13,14]. Surprisingly, these methods led to low order parameters which have been interpretated as indicating larger and slower motions must exist in addition to the fast and small amplitude motions determined from ^{15}N relaxation studies alone [15]. However, a recent study based on a refinement of the ubiquitin structure using a two site jump model has shown that the experimental RDCs can be interpreted using motions of smaller amplitudes [13,14,16]. In the following, we investigate and compare the effect

☆ This work was supported by an EMBO fellowship and by the European Union through the research Training Network "Cross-Correlation" for M.D. J.B. and I.D.C. acknowledge support from BBSRC and the Wellcome Trust, respectively.
* Corresponding author.
E-mail address: Michael.Deschamps@bioch.ox.ac.uk (M. Deschamps).

1090-7807/$ - see front matter © 2004 Elsevier Inc. All rights reserved.
doi:10.1016/j.jmr.2004.09.023

that specific types of intramolecular dynamics can have upon RDCs [12,15,17–27].

2. Method

The RDC (units Hz) between two nuclei I and S, that form a rigid dipolar inter-nuclear vector $\mathbf{v}$ (static model, Fig. 1A) and have a frequency difference $|\omega_I - \omega_S| \gg 2\pi J_{\text{obs}}$, where J_{obs} is the observed spectral splitting, is [7]:

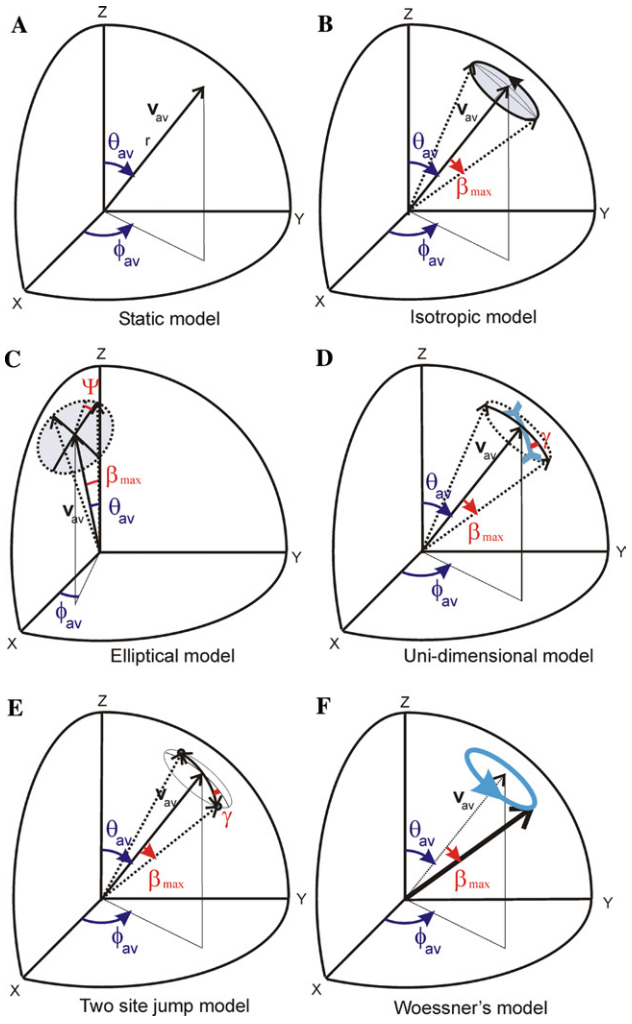

Fig. 1. The different models of local intramolecular dynamics are each represented on an octant of the unit sphere. The spherical polar coordinates θ_{av} and ϕ_{av} for the vector $\mathbf{v}_{\text{av}}$ corresponding to the average values of $\theta(\Gamma)$ and $\phi(\Gamma)$ are shown in a coordinate frame defined by the principal axis system (PAS) of the alignment tensor, **A**. The angle $\beta_{\max}$ is the maximum angle between $\mathbf{v}_{\text{av}}$ and $\mathbf{v}(\Gamma)$. In each case, the region on the sphere enclosed by the tip of the internuclear vector $\mathbf{v}(\Gamma)$ is highlighted in blue and the vibrationally averaged internuclear distance $\langle r\rangle$ is assumed to be constant. The various models are: (A) Static model. (B) Isotropic internal motion model: the vectors $\mathbf{v}(\Gamma)$ lie within a cone defined by the blue surface area. (C) Elliptical. (D) Uni-dimensional. (E) Two site jump. (F) Free diffusion of the internuclear axis about a fixed symmetry axis, Woessner's model.

$$RDC(\mathbf{v}) = D_a(3\cos^2\theta_{\text{av}} - 1) + \frac{3}{2}D_r\sin^2\theta_{\text{av}}\cos 2\phi_{\text{av}}, \quad (1)$$

where

$$D_a = -\frac{\gamma_I\gamma_S\hbar\mu_0 A_a(3\cos^2\Omega - 1)}{16\pi^2\langle r_{IS}^3\rangle}, \qquad D_r = RD_a \quad (2)$$

and

$$R = \frac{(A_{xx} - A_{yy})}{3A_a}, \qquad A_a = \frac{1}{3}\left(A_{zz} - \frac{A_{xx} + A_{yy}}{3}\right), \quad (3)$$

where R characterizes the rhombicity and A_a is the unitless axial component of the symmetric traceless molecular alignment tensor, **A**, in its principle axis system (PAS), θ_{av}, ϕ_{av} define the orientation of the dipolar inter-nuclear vector with respect to the PAS of the alignment tensor. $\langle r\rangle$ is the vibrationally averaged internuclear distance. Ω is the angle the restraint director makes with B_0, and in ideal solutions of bicelles and phages, it is $\pi/2$ and 0, respectively. We note also that a molecule possessing an anisotropic magnetic susceptibility, $\Delta\chi$, can adopt a weak preferential orientation in a magnetic field, B_0. However, the RDCs due to magnetic field induced orientation are usually small compared to samples dissolved in solutions of either bicelles or phages [8,28].

In the following we are interested in describing the effect of angular fluctuations on the RDC between two nuclei with spins $I = 1/2$. The effect of bond vibration upon the RDC will be neglected here, as it has been discussed elsewhere; it can be taken into account using a vibrationally averaged effective inter-nuclear distance $\langle r\rangle$ [33]. The orientation of a pair of nuclei, with respect to the PAS of the alignment tensor, **A** is described by a dipolar inter-nuclear vector $\mathbf{v}(\Gamma)$, where Γ represents one of the allowed conformations for this pair of nuclei. The angular fluctuations of the dipolar vector are described by an ensemble $\{\Gamma\}$ of allowed conformations, and assuming a constant energy potential function, the allowed conformations have equal probability. If interchange between conformations in the ensemble is rapid compared to any chemical shift differences exhibited by the ensemble, the NMR spectrum of each nucleus exhibits a single chemical shift, and the observed RDC is equal to the average RDC from each dipolar vector $\mathbf{v}(\Gamma)$ in the ensemble $\{\Gamma\}$ (see Eq. (4)). In the following, we have assumed that the PAS and the components D_a and D_r of the alignment tensor **A** remain fixed and invariant in the molecular frame, and that the local internal motions do not cause a significant change to the overall structure of the protein. With these assumptions, the RDC averaged over the ensemble is given by:

$$\begin{aligned}\langle RDC(\mathbf{v}(\Gamma))\rangle_\Gamma &= D_a(3\langle\cos^2\theta(\Gamma)\rangle_\Gamma - 1) \\ &\quad + \frac{3}{2}D_r\langle\sin^2\theta(\Gamma)\cos 2\phi(\Gamma)\rangle_\Gamma \\ &= D_a(3\langle z^2(\Gamma)\rangle_\Gamma - 1) + \frac{3}{2}D_r\langle x^2(\Gamma) \\ &\quad - y^2(\Gamma)\rangle_\Gamma \\ &= D_a\frac{\int\int_{\{\Gamma\}}(3z^2(\Gamma)-1)\,\mathrm{d}S}{\int\int_{\{\Gamma\}}\mathrm{d}S} + \frac{3}{2}D_r \\ &\quad \times \frac{\int\int_{\{\Gamma\}}x^2(\Gamma)-y^2(\Gamma)\,\mathrm{d}S}{\int\int_{\{\Gamma\}}\mathrm{d}S}, \end{aligned} \tag{4}$$

where $\mathrm{d}S$ is the elementary surface element of the region enclosed by the tip of the internuclear vector $\mathbf{v}\{\Gamma\}$. The vector $\mathbf{v}(\Gamma)$ can be defined using either spherical coordinates $(\theta(\Gamma),\phi(\Gamma))$ or cartesian coordinates $(x(\Gamma),y(\Gamma),z(\Gamma))$ in the PAS of the alignment tensor **A**. The average denoted by $\langle\rangle_\Gamma$ is the average formed from all of the allowed conformations, Γ, for a particular type of local internal motion. In the limit of a static structure Eq. (4) reduces to Eq. (1), and in the limit of complete random isotropic motion, the RDC tends to zero.

Several different types of angular fluctuations will be considered here, these are:

(a) Two-dimensional models: internal motion within a cone [8,12], Fig. 1B, and its anisotropic counterpart: Elliptical model [25], Fig. 1C.
(b) A uni-dimensional model of intra-molecular motion, Fig. 1D, which has two limiting cases which are referred to as vertical ($\gamma = 0$) and horizontal ($\gamma = \pi/2$) motions, respectively.
(c) The average RDC in the case of an equally populated two site jump model, where the inter-nuclear vector jumps by an angle $2\beta_{\max}$, Fig. 1E.
(d) The Woessner model of intra-molecular dynamics, which describes the free diffusion of the inter-nuclear dipolar vector about a fixed symmetry axis, Fig. 1F [34], is discussed in Appendix A.

For each dynamic model, the region on the unit sphere enclosed by the tip of the inter-nuclear vector $\mathbf{v}(\Gamma)$ is highlighted in blue in Fig. 1. In the following, we consider the linear average values θ_{av} and ϕ_{av} of $\theta(\Gamma)$, $\phi(\Gamma)$ over the ensemble of allowed conformations. The set of vectors $\mathbf{v}_{\mathrm{av}}$, $\mathbf{v}'(\beta)-\mathbf{v}_{\mathrm{av}}$, $\mathbf{v}''(\beta)-\mathbf{v}_{\mathrm{av}}$ describe the orientation of any internuclear vector $\mathbf{v}(\Gamma)=\mathbf{v}(\beta,\gamma)$ from the allowed conformations Γ where $\mathbf{v}(\beta,\gamma)$ is obtained from $\mathbf{v}'(\beta)=\mathbf{v}(\theta_{\mathrm{av}}+\beta,\ \phi_{\mathrm{av}})$ after a rotation by an angle γ about $\mathbf{v}_{\mathrm{av}}$, and $\mathbf{v}''(\beta)=\mathbf{v}(\beta,\pi/2)$ (see Fig. 2). This new vector is defined by

$$\begin{aligned}\mathbf{v}(\beta,\gamma) &= \cos\beta\mathbf{v}_{\mathrm{av}} + \sin\beta\cos\gamma(\mathbf{v}'(\beta)-\mathbf{v}_{\mathrm{av}}) \\ &\quad + \sin\beta\sin\gamma(\mathbf{v}''(\beta)-\mathbf{v}_{\mathrm{av}})\end{aligned} \tag{5}$$

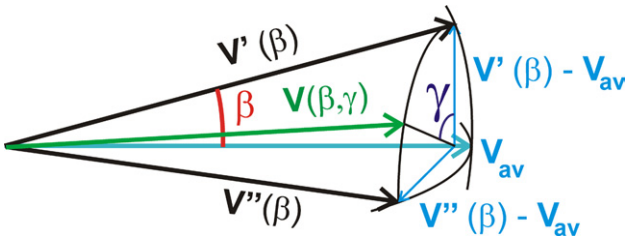

Fig. 2. A schematic diagram showing the interrelationship between the vectors $\mathbf{v}_{\mathrm{av}}$, $\mathbf{v}'(\beta)$, and the images formed by rotations through the angle γ or by $\pi/2$ about $\mathbf{v}_{\mathrm{av}}$, $\mathbf{v}(\beta,\gamma)$, and $\mathbf{v}''(\beta)$, respectively.

with

$$\begin{aligned}\mathbf{v}'(\beta)-\mathbf{v}_{\mathrm{av}} &= (x',y',z') = (\cos\theta_{\mathrm{av}}\cos\phi_{\mathrm{av}}, \cos\theta_{\mathrm{av}}\sin\phi_{\mathrm{av}}, -\sin\theta_{\mathrm{av}}), \\ \mathbf{v}''(\beta)-\mathbf{v}_{\mathrm{av}} &= (x'',y'',z'') = (-\sin\phi_{\mathrm{av}}, \cos\phi_{\mathrm{av}}, 0).\end{aligned} \tag{6}$$

3. Results for different models of motional averaging

3.1. Isotropic internal motion [8,12,24]

For isotropic internal motion (diffusion in a cone of semi-angle $\beta_{\max}$), the average is obtained using Eqs. (4) and (5) and the limits $\{\Gamma\} = \{\mathbf{v}(\beta,\gamma)/\beta \in [0;\beta_{\max}],\ \gamma \in [0;2\pi],\ \text{where } 0^\circ \leqslant \beta_{\max} \leqslant 180^\circ\}$. The values of $x(\Gamma)$, $y(\Gamma)$, and $z(\Gamma)$ are derived from Eq. (5), and the resulting RDC is given by [8,12,24]:

$$\begin{aligned}\langle RDC\rangle_\Gamma &= \frac{\cos\beta_{\max}+\cos^2\beta_{\max}}{2}\left[D_a(3\cos^2\theta_{\mathrm{av}}-1)\right. \\ &\quad \left. + \frac{3}{2}D_r\sin^2\theta_{\mathrm{av}}\cos 2\phi_{\mathrm{av}}\right] \\ &= S_{\mathrm{iso}}(\beta_{\max}) \times RDC(\mathbf{v}_{\mathrm{av}}).\end{aligned} \tag{7}$$

Compared to the static model, Eq. (1), this particular model of local internal motion gives rise to RDCs with a similar functional form except that they are scaled by the factor $S_{\mathrm{iso}}(\beta_{\max})$. $S_{\mathrm{iso}}(\beta_{\max})$ has a similar functional form to the order parameter $S^{\mathrm{LS}}_{\mathrm{cone}} = (S^{\mathrm{LS}\ 2}_{\mathrm{cone}})^{1/2}$, where $(S^{\mathrm{LS}}_{\mathrm{cone}})^2$ is the order parameter commonly used for describing NMR relaxation behaviour [12]. The curve $S_{\mathrm{iso}}(\beta)$ is shown in Fig. 3; in contrast to the order parameter $(S^{\mathrm{LS}}_{\mathrm{cone}})^2$ describing autocorrelated relaxation processes, it can, in some motional regimes exhibiting large amplitude, adopt negative values. When the cone is extended to either the whole half-sphere, i.e., $\beta_{\max} = 90^\circ$ or the entire sphere, i.e., $\beta_{\max} = 180^\circ$, the RDC vanishes. However, unlike $S_{\mathrm{iso}}(\beta)$, the order parameter $(S^{\mathrm{LS}}_{\mathrm{cone}})^2$ describing relaxation behaviour is generally only affected by motions which are faster than the rotational correlation time [24]. In principle the order parameter $S_{\mathrm{iso}}(\beta_{\max})$ could also be affected by local motions occurring on much slower time scales than those affecting $(S^{\mathrm{LS}}_{\mathrm{cone}})^2$. If $S_{\mathrm{iso}}(\beta_{\max})$ is assigned the value 0.95 $(S^2_{\mathrm{iso}}(\beta_{\max}) = 0.9025)$, then $\beta_{\max} = 15^\circ$. Molecular dynamics studies [24] have indicated that this motional model with $\beta_{\max}$ having a

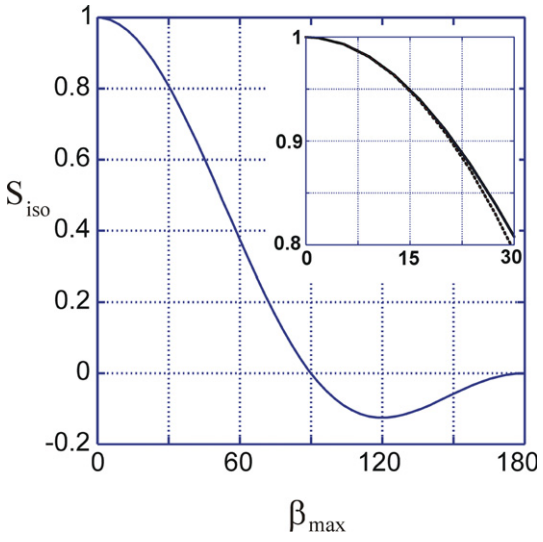

Fig. 3. The function $S_{iso}(\beta_{max}) = (\cos\beta_{max} + \cos^2\beta_{max})/2$, as a function of the angle β_{max}. An expansion of the initial portion of this curve and its Taylor expansion (dashed line) are shown in the upper right hand corner, demonstrating the good agreement between each curve whenever $0° \leqslant \beta_{max} \leqslant 20°$.

value of approximately 15° is relevant for the structured parts of proteins, although the model might not be suitable for mobile regions such as loop or tail regions. Average GAF amplitudes of 14.4–17° have been determined for secondary structure elements with single N–^{N}H RDC data sets, in combination with high-resolution structural models (X-ray structure with a resolution of 0.9 Å) [26]. Recent studies have determined values for $S^2_{iso}(\beta_{max})$ as low as 0.4–0.6 using measurements of RDCs in multiple alignment media [14] or by sampling different internuclear dipolar vectors [13]. These values correspond to $S_{iso}(\beta_{max})$ between 0.63 and 0.77, leading to β_{max} approximatively in the range of 43 and 33°, respectively. Anticipating the results of future sections it is helpful to express $\sin\beta_{max}$, $\cos\beta_{max}$, and $\cos^2\beta_{max}$ using the approximate Taylor series expansions: $\sin\beta_{max} \approx \beta_{max}$, $\cos\beta_{max} \approx 1 - \beta^2_{max}/2$, $\cos^2\beta_{max} \approx 1 - \beta^2_{max}$. Assuming β_{max} lies within the range $0° \leqslant |\beta_{max}| \leqslant 20°$ these approximate series expansions are accurate to within ~0.5% and $S_{iso}(\beta_{max})$ can then be written as $S_{iso}(\beta_{max}) \approx 1 - 3\beta^2_{max}/4$. A comparison of the values for $S_{iso}(\beta_{max})$ obtained from these two forms as a function of β_{max} is shown in the expansion in Fig. 3. After employing these Taylor series expansions, Eq. (7) can be written as:

$$\begin{aligned}\langle RDC\rangle_\Gamma &= RDC(\mathbf{v}_{av}) + \Delta^{RDC}_{dyn}\\ &\approx D_a(3\cos^2\theta_{av} - 1) + \frac{3}{2}D_r\sin^2\theta_{av}\cos 2\phi_{av}\\ &\quad - \frac{3\beta^2_{max}}{4}\left[D_a(3\cos^2\theta_{av} - 1) + \frac{3}{2}D_r\sin^2\theta_{av}\cos 2\phi_{av}\right],\end{aligned} \tag{8}$$

where the first part of Eq. (8), RDC($\mathbf{v}_{av}$), is the RDC expected in the case of no local internal motion, Eq. (1), and the second portion, Δ^{RDC}_{dyn}, represents the contribution that this model of local internal dynamics makes to the RDC.

3.2. Elliptical model [25]

A new model for internal motion has recently been proposed, which corresponds to diffusion in a cone having an elliptical section of maximum semi-angle β_{max}, eccentricity e ($e = 0$ corresponds to spherical symmetry and $e = 1$ to a unidimensional model), if the major axis of the ellipse is parallel to $\mathbf{v}(\beta,\psi) - \mathbf{v}_{av}$, Eq. (5) is written as:

$$\begin{aligned}\mathbf{v}(\beta,\gamma) &= \sqrt{\cos^2\beta + e^2\sin^2\gamma\sin^2\beta}\,\mathbf{v}_{av}\\ &\quad + \cos\gamma\sin\beta\,\mathbf{v}(\beta,\psi)\\ &\quad + \sin\gamma\sin\beta\sqrt{1-e^2}\,\mathbf{v}(\beta,\psi+\pi/2)\end{aligned} \tag{9}$$

and using the integration limits $\Gamma = \{\beta \in [0;\beta_{max}], \gamma \in [0;2\pi]\}$ and $0° \leqslant \beta_{max} \leqslant 20°$, Eq. (4) becomes:

$$\begin{aligned}\langle RDC\rangle_\Gamma &= D_a\frac{\int_0^{2\pi}\int_0^{\beta_{max}}[3z^2(\Gamma)-1]r(\beta,\gamma)\,d\beta\,d\gamma}{\int_0^{2\pi}\int_0^{\beta_{max}} r(\beta,\gamma)\,d\beta\,d\gamma}\\ &\quad + \frac{3}{2}D_r\frac{\int_0^{2\pi}\int_0^{\beta_{max}}[x^2(\Gamma)-y^2(\Gamma)]r(\beta,\gamma)\,d\beta\,d\gamma}{\int_0^{2\pi}\int_0^{\beta_{max}} r(\beta,\gamma)\,d\beta\,d\gamma},\end{aligned} \tag{10}$$

where the parameter $r(\beta,\gamma)$ is defined to be:

$$r(\beta,\gamma) = \sin\beta\sqrt{1-e^2\sin^2\gamma} \tag{11}$$

and the values of $x(\Gamma)$, $y(\Gamma)$, and $z(\Gamma)$ are derived from Eq. (9). Using the Taylor series expansions for the angles shown above and performing the calculation shown in Eq. (10) with MAPLE, the average RDC is found to be:

$$\begin{aligned}\langle RDC\rangle_\Gamma &= RDC(\mathbf{v}_{av}) + \Delta^{RDC}_{dyn}\\ &\approx D_a(3\cos^2\theta_{av} - 1) + \frac{3}{2}D_r\sin^2\theta_{av}\cos 2\phi_{av}\\ &\quad + \beta^2_{max}\left[\frac{D_a}{2e^2}\left[2e^4 - 4e^2 + \sin^2\theta_{av}(-1+7e^2\right.\right.\\ &\quad -4e^4 + 2\cos^2\psi(1-e^2+e^4)) + \frac{K(e)}{E(e)}(1-e^2)\\ &\quad \left.\times(e^2 + \sin^2\theta_{av}(1-2e^2+\cos^2\psi(e^2-2)))\right]\\ &\quad + \frac{D_r}{4e^2}\left[(e^4 - e^2 + 1)\times(-2\sin 2\psi\cos\theta_{av}\sin 2\phi_{av}\right.\\ &\quad +2\cos 2\psi\cos 2\phi_{av} - \cos 2\psi\sin^2\theta_{av}\cos 2\phi_{av})\\ &\quad +3(e^4 - 2e^2)\sin^2\theta_{av}\cos 2\phi_{av} + \frac{K(e)}{E(e)}(1-e^2)\\ &\quad \times\left((2-e^2)(\cos 2\psi\sin^2\theta_{av}\cos 2\phi_{av}/2\right.\\ &\quad -\cos 2\psi\cos 2\phi_{av} + \sin 2\psi\cos\theta_{av}\sin 2\phi_{av})\\ &\quad \left.\left.\left.+3e^2\sin^2\theta_{av}\cos 2\phi_{av}/2\right)\right]\right],\end{aligned} \tag{12}$$

where $K(k)$ and $E(k)$ are complete elliptic integrals of the first and second kind for which the modulus

$k = e$, and where $K(0) = E(0) = \pi/2$, $E(1) = 1$ and $\lim_{e \to 1} K(e) = \infty$, but $\lim_{e \to 1}(1 - e^2)K(e)/E(e) = 0$. The elliptical model is relevant according to MD trajectories [24]. However, this function is very complex, and further discussion will be limited to two limiting cases: (1) The isotropic motional model, Eq. (8), is obtained when $e = 0$, and (2) A uni-dimensional motional model arises when $e = 1$, and is described in the next section.

3.3. Uni-dimensional motion ($e = 1$)

In the following, we assume uni-dimensional motion where the inter-nuclear vector is located on a circular arc whose two ends are described by the vectors $\mathbf{v}(\beta_{\max}, \gamma)$ and $\mathbf{v}(\beta_{\max}, \gamma + 180°)$, with $0° \leqslant |\beta_{\max}| \leqslant 20°$. This corresponds to the limit $e = 1$ of the elliptical motion when $\psi = \gamma$ (see Fig. 1). With these assumptions the dynamically averaged RDC can be expressed using Eq. (12) as the sum of a static and a dynamic contributions, Eq. (13):

$$\begin{aligned}\langle RDC\rangle_{\Gamma_{\text{Uni-dim}}} &= RDC(\mathbf{v}_{\text{av}}) + \Delta_{\text{dyn}}^{\text{RDC}} \\ &\approx D_a\left[(3\cos^2\theta_{\text{av}} - 1) + \frac{3}{2}R\sin^2\theta_{\text{av}}\cos 2\phi_{\text{av}}\right] \\ &\quad + \frac{\beta_{\max}^2}{3}D_a\left[3(\cos^2\gamma\sin^2\theta_{\text{av}} - \cos^2\theta_{\text{av}})\right. \\ &\quad + \frac{3}{2}R(\cos 2\phi_{\text{av}}(\cos^2\gamma\cos^2\theta_{\text{av}} - \sin^2\theta_{\text{av}} \\ &\quad \left.-\sin^2\gamma) - \sin 2\gamma\sin 2\phi_{\text{av}}\cos\theta_{\text{av}})\right]. \qquad (13)\end{aligned}$$

The first part of Eq. (13), $RDC(\mathbf{v}_{\text{av}})$, is the RDC expected in the case of no local internal motion, Eq. (1), and the second portion, $\Delta_{\text{dyn}}^{\text{RDC}}$, represents the contribution that this unusual and restricted type of local internal dynamics makes to the RDC. The dynamical contribution to the averaged RDC is proportional to $\beta_{\max}^2/3$, and for the two specific cases where $\gamma = 0$ (vertical model) and $\gamma = \pi/2$ (horizontal model), the averaged RDCs are given by

$\gamma = 0$,

$$\begin{aligned}\langle RDC\rangle_{\Gamma_{\text{vertical}}} &\approx D_a\left[(3\cos^2\theta_{\text{av}} - 1) + \frac{3}{2}R\sin^2\theta_{\text{av}}\cos 2\phi_{\text{av}}\right] \\ &\quad - \beta_{\max}^2 D_a\left[\cos 2\theta_{\text{av}} - \frac{3}{2}R\frac{\cos 2\theta_{\text{av}}\cos 2\phi_{\text{av}}}{3}\right], \qquad (14)\end{aligned}$$

$\gamma = \pi/2$,

$$\begin{aligned}\langle RDC\rangle_{\Gamma_{\text{horizontal}}} &\approx D_a\left[(3\cos^2\theta_{\text{av}} - 1) + \frac{3}{2}R\sin^2\theta_{\text{av}}\cos 2\phi_{\text{av}}\right] \\ &\quad - \beta_{\max}^2 D_a\left[\cos^2\theta_{\text{av}} + \frac{3}{2}R\frac{(1 + \sin^2\theta_{\text{av}})\cos 2\phi_{\text{av}}}{3}\right]. \qquad (15)\end{aligned}$$

If it is assumed that isotropic and unidimensional motions can occur independently for the same inter-nuclear vector, the individual motional models, Eqs. (7) and (13), can be superimposed and this type of model could be used for describing a specialised form of anisotropic motion [25]. In this case, the averaged RDC is given by:

$$\begin{aligned}\langle RDC\rangle_{\text{iso+uni-dim}} &= S_{\text{iso}}RDC(\mathbf{v}_{\text{av}}) \\ &\quad + S_{\text{iso}}(\Delta_{\text{dyn}}^{\text{RDC}})_{\text{uni-dim}}, \qquad (16)\end{aligned}$$

where $S_{\text{iso}} = (\cos\beta_{\max} + \cos^2\beta_{\max})/2$.

3.4. Two-site jump model exhibiting equal populations

The averaged RDC can also be quantitatively expressed in the case of a two site equally populated jump model where each inter-nuclear vector jumps by the angle $2\beta_{\max}$, where $0° \leqslant |\beta_{\max}| \leqslant 20°$, and the ensemble inter-converts at a rate fast compared to any chemical shift differences. The average orientation is again described by $\mathbf{v}_{\text{av}}$, the two sites are described by the vectors $\mathbf{v}(\beta_{\max}, \gamma)$ and $\mathbf{v}(\beta_{\max}, \gamma + 180°)$, and the angle between the axis of the jump and the axis of vertical motion is as shown in Figs. 1E and 2. With these assumptions the dynamically averaged RDC is found to be:

$$\begin{aligned}\langle RDC\rangle_{\Gamma_{\text{2sites}}} &= \frac{1}{2}[RDC(\mathbf{v}(\beta_{\max}, \gamma)) + RDC(\mathbf{v}(\beta_{\max}, \gamma + 180°))] \\ &\approx D_a\left[(3\cos^2\theta_{\text{av}} - 1) + \frac{3}{2}R\sin^2\theta_{\text{av}}\cos 2\phi_{\text{av}}\right] \\ &\quad + \beta_{\max}^2 D_a\left[3(\cos^2\gamma\sin^2\theta_{\text{av}} - \cos^2\theta_{\text{av}}) + \frac{3}{2}R\right. \\ &\quad \times(\cos 2\phi_{\text{av}}(\cos^2\gamma\cos^2\theta_{\text{av}} - \sin^2\theta_{\text{av}} - \sin^2\gamma) \\ &\quad \left.- \sin 2\gamma\sin 2\phi_{\text{av}}\cos\theta_{\text{av}})\right]. \qquad (17)\end{aligned}$$

The dynamical contribution to the exchange averaged RDC is proportional to $\beta_{\max}^2$, and for the two specific cases where $\gamma = 0$ (vertical exchange jump model) and $\gamma = \pi/2$ (horizontal exchange jump model), the exchange averaged RDCs are given by:

$\gamma = 0$,

$$\begin{aligned}\langle RDC\rangle_{\Gamma_{\text{2sites}}} &\approx D_a\left[(3\cos^2\theta_{\text{av}} - 1) + \frac{3}{2}R\sin^2\theta_{\text{av}}\cos 2\phi_{\text{av}}\right] \\ &\quad - 3\beta_{\max}^2 D_a\left[\cos 2\theta_{\text{av}} - \frac{3}{2}R\frac{\cos 2\theta_{\text{av}}\cos 2\phi_{\text{av}}}{3}\right], \qquad (18)\end{aligned}$$

$\gamma = \pi/2$,

$$\begin{aligned}\langle RDC\rangle_{\Gamma_{\text{2sites}}} &\approx D_a\left[(3\cos^2\theta_{\text{av}} - 1) + \frac{3}{2}R\sin^2\theta_{\text{av}}\cos 2\phi_{\text{av}}\right] \\ &\quad - 3\beta_{\max}^2 D_a\left[\cos^2\theta_{\text{av}} + \frac{3}{2}R\frac{(1 + \sin^2\theta_{\text{av}})\cos 2\phi_{\text{av}}}{3}\right]. \qquad (19)\end{aligned}$$

Compared to the continuous ensemble uni-dimensional model described in Section 3.3, Eqs. (13)–(15), the RDC averaged by two-site-exchange is seen to be three times more sensitive to motion. The factor of three occurs because Eq. (17) is formed from a linear average of two contributions having equal magnitude, with each proportional to $\beta_{\max}^2$, e.g., $[\beta^2+(-\beta)^2]/2=\beta^2$, whereas Eqs. (13)–(15) are developed using continuous averages employing integrals of the type $\langle\beta^2\rangle=\int_{-\beta}^{\beta}u^2\,du/2\beta=\beta^2/3$. Consequently, $\beta_{\max}$ values derived using this two site jump model need to be increased by $\sqrt{3}$ for them to be comparable with values derived from Eqs. (13)–(15). For a system undergoing independent vertical and horizontal uni-dimensional two site exchange simultaneously (4-site jump), the dynamically averaged RDC is given by Eq. (20):

$$\langle RDC(\mathbf{v}(\beta,0))\rangle_{\Gamma_{2\text{sites}}}+\langle RDC(\mathbf{v}(\beta,\pi/2))\rangle_{\Gamma_{2\text{sites}}}/2 \approx\left(1-\frac{3}{2}\beta_{\max}^2\right)D_a\left[(3\cos^2\theta_{\text{av}}-1)+\frac{3}{2}R\sin^2\theta_{\text{av}}\cos 2\phi_{\text{av}}\right]. \tag{20}$$

It is known that for autocorrelated dipole–dipole relaxation with constant inter-nuclear distance the order parameter S^2 describing an equally populated two site jump model, with jump angle $2\beta_{\max}$ is given by $S^2=(3\cos^2 2\beta_{\max}+1)/4$ [12]. Expanding this trigonometric function in a Taylor series and truncating at the first term, as discussed earlier, leads to $S^2=1-3\beta_{\max}^2$, which is a good approximation provided $0^\circ\leqslant|\beta_{\max}|\leqslant 20^\circ$. Identifying the function $1-3\beta_{\max}^2/2$ in Eq. (20) with a similar order parameter S gives $S^2=1-3\beta_{\max}^2$ which has a similar functional form to the order parameter used for exchange averaged autocorrelated dipole–dipole relaxation. The model of free diffusion about a fixed symmetry axis, or Woessner's model, and its link to the two-site jump model is treated in Appendix A and a discussion about the effects of motional averaging on the distribution of RDCs is also included in Appendix B.

4. Models of motional averaging and the differential effect upon individual RDCs

Several studies[15,18–21,25] have indicated that, at room temperature, fast vibrations or librations of the protein backbone NH vector occur with angular amplitudes of about 15–20°. In a coordinate frame attached to the peptide plane the angular amplitudes of in-plane and out-of-plane NH vector vibrations are thought to be between 3–5° and 10–12°, respectively [19,22,23]. Simulations of the effects of the different types of intra-molecular dynamics upon the calculated RDCs, compared to the static model, are shown in Fig. 4 for two different values of R as a function of θ_{av}. In each case, the amplitude of motion was assumed to be similar with $\beta_{\max}=15^\circ$ and $D_a=1$ Hz. The largest change to the dynamically averaged RDC is approximately ±0.1 Hz or about ±5% of the maximum static value of 2 Hz, Fig. 4D. These calculations suggest that the magnitude of an RDC is not particularly sensitive to small amplitude motions or librations ($|\beta_{\max}|\leqslant 15^\circ$) and a detailed analysis of these small motions from measurements of individual RDC values will require precise measurements in addition to the requirement for an accurate knowledge of the magnitude of the alignment tensor, **A** (see later sections). In the case of the vertical motional model, the influence upon the RDC is proportional to $\cos 2\theta_{\text{av}}$ and any motional effect will vanish whenever $\theta_{\text{av}}=45^\circ$ or 135°. For the vertical and horizontal models, the correction term $\Delta_{\text{RDC}}^{\text{dyn}}$ will be modulated by the angle γ whenever the motion is anisotropic [29]. The difference between curves (B and E) and (C and F) are quite small, which might explain why anisotropic

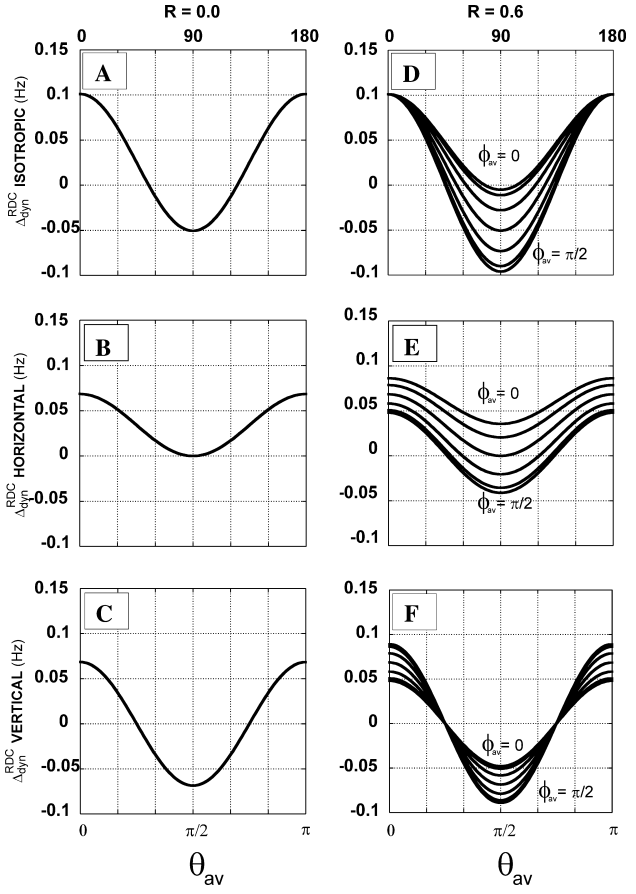

Fig. 4. The magnitude of $\Delta_{\text{dyn}}^{\text{RDC}}$ due to local motions as a function of θ_{av} and ϕ_{av}. $\Delta_{\text{dyn}}^{\text{RDC}}$ for curves a and d (isotropic) is defined as the difference between Eq. (1) and the RDC calculated using Eq. (7) for isotropic motion. $\Delta_{\text{dyn}}^{\text{RDC}}$ (vertical) for curves c and f, and $\Delta_{\text{dyn}}^{\text{RDC}}$ (horizontal) for curves b and e, are calculated using either Eq. (14) or Eq. (15). $\Delta_{\text{dyn}}^{\text{RDC}}$ is plotted as a function of θ_{av} for six values of ϕ_{av} (0, 15, 30, 45, 60, 75, and 90) assuming $\beta_{\max}=15^\circ$ in each case. $D_a=1$ Hz and R is either 0.0 (A–C) or 0.6 (D–F).

motion is difficult to determine, and none of the motions currently predicted by molecular dynamics features large degrees of anisotropy. The different models give rise to slightly different motional effects as expected, but the differences are typically fairly small.

5. The effect of motional averaging upon the determination of θ_{av} and ϕ_{av} from an individual RDC: the effect of R^{obs}

It has been shown for a few proteins that a single structure representation is sufficient to fit the RDCs within the experimental errors [16,30]. This is true when S_{iso} is nearly constant for the ensemble of inter-nuclear vectors, and in such a case the error on R^{obs}, the observed value of R, will often be small (see Appendix B).

We consider here the case when there is some anisotropic motion, and when the rhombicity R is different from 0. In this case, motional averaging influences the value of R^{obs} determined from the distribution of RDCs and affects the back-calculation of θ_{av} and ϕ_{av} from an individual RDC (i.e., using one alignment tensor). A more detailed analysis of some additional consequences of motional averaging upon back calculated values of θ_{av} and ϕ_{av} from an individual RDC is shown in Appendix C.

Each model for motional averaging has a slightly different influence upon the value of R determined from a distribution of RDCs, R_{obs} (see Appendix B). Insight into the influence that R^{obs} exerts upon the back-calculated angles can be explored by assuming that instead of motion being the influence upon the *RDC* the internuclear vector remains static, in a distribution with rhombicity R^{obs}, but is given a new orientation. The new orientation can be defined using either a vertical, $\Delta\theta$, or an azimuthal, $\Delta\phi$, angular displacement as shown by Eqs. (21) and (22).

$$RDC^{exp} = D_a\left[(3\cos^2(\theta_{av}+\Delta\theta)-1) + \frac{3}{2}R^{obs}\sin^2(\theta_{av}+\Delta\theta)\cos^2\phi_{av}\right], \quad (21)$$

$$RDC^{exp} = D_a\left[(3\cos^2(\theta_{av}-1) + \frac{3}{2}R^{obs}\sin^2\theta_{av}\cos 2(\phi_{av}+\Delta\phi)\right]. \quad (22)$$

In these equations RDC^{exp} is calculated, via Eq. (1), for orientation (θ_{av}, ϕ_{av}), employing values for D_a and R assuming a static distribution (see Fig. 5). R^{obs} represents the value for R assuming motional averaging of the distribution of RDCs. The angular displacements $\Delta\theta$ and $\Delta\phi$ are the small changes necessary to the polar angles (θ_{av}, ϕ_{av}) so as to give the value RDC^{exp} when using R^{obs}. Employing $D_a = 1$ Hz, $R = 0.3$, and $R^{obs} = 1.05R$ the displacement angles vary within the range of $\Delta\theta = \pm 4.6°$ and $\Delta\phi = \pm 8.9°$; the results are shown in Figs. 5A and B. The main influence of R^{obs} upon θ_{av} is limited to those internuclear vectors lying close to the equatorial plane and, furthermore, for these vectors the effect upon ϕ_{av} can be quite significant if ϕ_{av} happens to be close to 0, 90, 180 or 270°. Consequently, the error introduced by different values for R^{obs} is usually going to be quite small. However, for those internuclear vectors close to the equatorial plane and which have the special ϕ_{av} angles discussed above, the back calculated orientation may be affected by an error on the rhombicity.

6. Other factors influencing the magnitude of a RDC

The above analysis has revealed situations where local internal dynamics ($\beta_{max} \leqslant 20°$) can influence the magnitude of a RDC by ~5%. It is, therefore, of interest to briefly highlight other effects influencing the magnitude of RDCs such as those from the NMR measurement process or from the assumption of uniform interatomic distances for similar atom pairs. The precision of each resonance frequency after Fourier transformation of a time domain signal is strongly influenced by S/N ratio, linewidth, interpoint digital resolution, and truncation artefacts [31,32]. Hence, extracting RDCs from direct time domain fitting of constant time datasets is sometimes advantageous [33]. A relatively small error of 10% to 180° pulse widths has been shown to decrease experimental C^{α}–H^{α} splittings by ~0.5 Hz (~0.3% assuming $J(C^{\alpha}–H^{\alpha}) \approx 140$ Hz). The partial cancellation of cross-correlation effects and the contribution of several RDCs to the same splitting, such as H^{α}–H^{N} when the N–H^{N} splitting is measured, also causes small errors [35]. Anisotropy in J is reported to be very small for N–H^{N}, C^{α}–H^{α}, and H^{α}–H^{N} couplings although it has been calculated to be of the order of 0.45% and 0.51% of the observed RDCs for C^{α}–C′ and C′–N spin pairs [32,35]. The assumption of a uniform vibrationally averaged internuclear distance is an important influence in quantitative analysis of RDCs. The high resolution X-ray structure of crambin (1EJG.pdb, $R = 0.54$ Å) reports a RMSD of bond lengths from ideal values of 0.023 Å [36]. Assuming this degree of variability exists in solution it would influence the RDCs with approximately the same order of magnitude as that of low amplitude ($\beta_{max} \leqslant 20°$) internal motion. Another small but interesting effect comes from the intrinsic precision of a pdb file, where each coordinate is typically reported with a precision of 5×10^{-4}. Hence, there is always an uncertainty in the interatomic distance and thus in the RDC of at least ~0.5% (for RDCs of 20 Hz this corresponds to 0.1 Hz) due to the truncation of atomic coordinates.

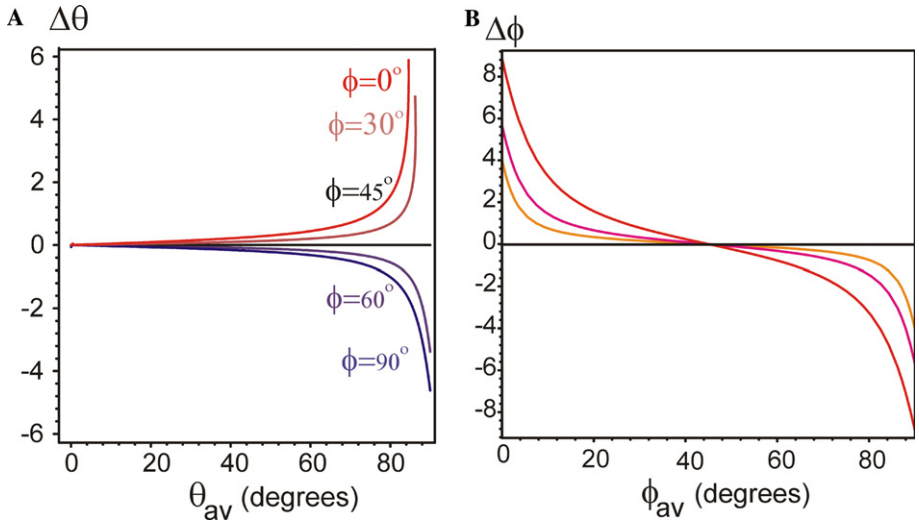

Fig. 5. (A) The required variation to the angle θ_{av}, $\Delta\theta$, in order to maintain the equality of Eq. (21) as a function of θ_{av} when R^{obs} is assigned the value $1.05 \times R$. RDC^{exp} was computed using Eq. (1) and ϕ_{av} was assigned values of 0°, 30°, 45°, 60°, and 90°. For $\phi_{av} = 45°$, the rhombic term vanishes and $\Delta\theta$ is zero. (B) The required variation to the angle ϕ_{av}, $\Delta\phi$, in order to maintain the equality of Eq. (22) as a function of ϕ_{av} when using the values for R^{obs} of $1.01 \times R$ (yellow), $1.02 \times R$ (pink) or $1.05 \times R$ (red). In each case only 8.3, 15.9, and 29.7% of the vectors are found to require a value for $\Delta\phi$ greater than 1°.

The effects of vertical and horizontal angular displacements of 1°, 2°, and 3° upon the magnitude of a RDC compared to the RDC from a static structure as a function of θ_{av} and ϕ_{av} are shown in Fig. 6. For $\theta_{av} = 45°$ and $\phi_{av} = 90°$ ($RDC = 0.275$ Hz), effects as high as -0.06 Hz can be seen for a vertical angular shift of 1°, corresponding to 21.8% of the theoretical RDC. Vertical rather than horizontal angular shifts are found to lead greater effects. Moreover, the angular deviations of X-ray structures have been noted to induce systematic errors to an alignment tensor calculated with singular value decomposition [37].

7. Conclusion

The effect upon RDCs of three new models for motional averaging (elliptic [25], uni-dimensional and equally populated two site jump) and three established models (static, isotropic motion in a cone and free diffusion about a fixed symmetry axis: Woessner's model) have been compared assuming that the amplitude of motion in each case, $\beta_{max} \leqslant 15$–$20°$. Whenever $\beta_{max} \leqslant 20°$, the impact of the different motional models upon individual RDCs is fairly similar and compared to a static model the RDC can be reduced by up to $\approx \pm 5\%$; however, since the motional effects are proportional to β^2_{max} they will increase rapidly with increasing amplitude. Furthermore, in the limit that $\beta_{max} \leqslant 20°$ differential effects between the commonly assumed motional model of isotropic diffusion in a cone and either the elliptic or the uni-dimensional motional models are also quite small at $\approx < 5\%$ (Section 4). Compared to the continuous uni-dimensional model, the RDC averaged by two-site-exchange is three times more sensitive to motion, and, consequently, β_{max} values derived using a two site jump model need to be increased by $\sqrt{3}$ to be comparable with values derived using a continuous uni-dimensional model.

Assuming a static model and a small error of only 5% in the rhombicity value R^{obs}, the experimental value of R, this small error is found to have an impact upon the back calculation of the angles θ_{av} and ϕ_{av}. These angles define the orientation of an internuclear vector in the PAS of **A** and especially for those internuclear vectors lying in or close to the equatorial plane the 5% error in R can translate into angular errors for θ_{av} and ϕ_{av} of up to $\pm 5°$ or $\pm 9°$, respectively when assuming $R^{obs} = 1.05R$ and $R = 0.3$ (Section 5). Section 6 considers a few experimental and intrinsic molecular properties each of which is expected to give rise to only a relatively small influence upon an experimental RDC. Also considered in Section 6 is the effect that either a small vertical or a small horizontal angular atomic displacement has upon a RDC. For instance, assuming a static motional model, and for relatively small vertical angular deviations, of only 3°, quite significant changes of up to $\approx 9\%$ of the maximum RDC can arise. This simple calculation gives some insight into the effect upon a RDC that a molecular structure exhibiting coordinate error may exert. Motion influences the upper and lower bounds of the distribution of RDCs and in the case that the alignment tensor **A** exhibits rhombicity, R, the experimental estimate of the rhombicity, R^{obs}, from the distribution of RDCs can lead to quite large errors in the estimate of R which may be up to $\approx 14\%$ in the

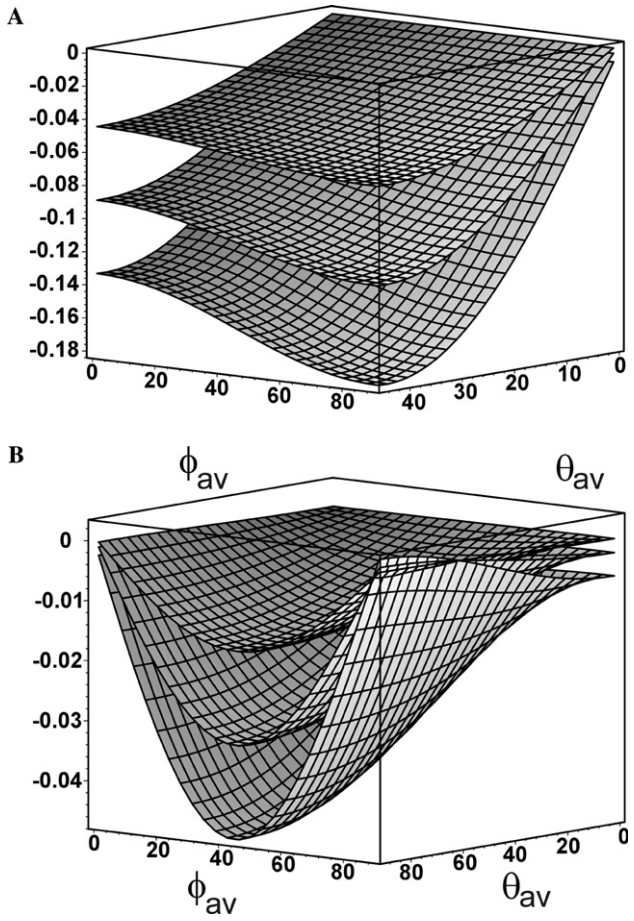

Fig. 6. Plots of the difference between a static *RDC* having an orientation defined by the polar angles (θ_{av}, ϕ_{av}) and that obtained after a vertical (A) or a horizontal (B) displacement equivalent to either 1°, 2° or 3° employing $D_a = 1$ Hz and $R = 0.3$. These surfaces compare the effect of angular displacements and the experimental error on the measured RDC.

case of vertical uni-dimensional motion (second table of Appendix B.2). These conclusions were formed from simulations which used distributions of RDCs composed of 6316 internuclear vectors where the upper and lower bounds of the distribution are well defined, however, many fewer RDCs are measured in an experiment in which case the upper and lower bounds are much less well defined possibly leading to some additional error in R^{obs}.

Appendix A. Free diffusion about a fixed symmetry axis

For the particular motion shown in Fig. 1F, which describes the free diffusion of the inter-nuclear axis about a fixed symmetry axis, the angle β is constant and set to β_{max}, and is the angle between the internuclear axis and the symmetry axis. No Taylor series expansion is needed, hence $0° \leqslant |\beta_{max}| \leqslant 180°$, and the observed RDC is given by

$$\langle RDC \rangle_{\Gamma} = \frac{(3\cos^2\beta_{max} - 1)}{2} \times RDC(\mathbf{v}_{av}). \quad (A.1)$$

For a CH vector in an idealised methyl group, the angle β_{max} (C–C–H angle) is approximately 111° [34], and the scaling factor $P_2(\cos\beta_{max})$ becomes −0.31.

We note that if the result from Eq. (17) is averaged over the angle γ (where γ varies between 0 and 2π), the exchange averaged RDC $\langle\langle RDC\rangle_{\Gamma_{2sites}}\rangle_{\gamma}$ is scaled by the factor $(1 - 3\beta_{max}^2/2)$ rather than simply containing a term proportional to β_{max}^2. It is useful to perform this calculation because, for a uniform ensemble of internuclear vectors exhibiting two site exchange, jumping by a fixed angle $2\beta_{max}$ (within the limits $0° \leqslant \beta_{max} \leqslant 20°$) and exhibiting a variable angle γ (see Fig. 1E), the process of averaging over the angle γ becomes equivalent to free diffusion about a fixed symmetry axis if the angle β_{max} is identified with the angle between the diffusion axis and each internuclear vector. This new scaling factor agrees with that of Eq. (21), when a Taylor series expansion is applied to $\cos^2\beta_{max}$, leading to $(3\cos^2\beta_{max} - 1)/2 \approx 1 - 3\beta_{max}^2/2$. Employing these arguments, a connection can be made between a continuous two site jump model of section 3D and Woessner's dynamic model.

Appendix B. Motional averaging and the effect upon the distribution of RDCs

The effect of the angular fluctuations upon the distribution of the RDCs is compared for the different dynamic models. The distribution of RDCs is important because, for a protein of unknown structure, it is used to determine the parameters D_a^{obs} and R^{obs} that characterise the alignment tensor, **A**. In the following sections, D_a^{obs} and R^{obs} correspond to the values of D_a and R inferred from a distribution of RDC values.

B.1. Remarks on RDC distributions

It has been pointed out [38] that the magnitude of the alignment tensor **A** determined from a distribution of RDCs depends not only upon the number of available dipolar vectors but also upon the uniformity of their distribution. In general it is quite difficult accurately to determine the upper bound of the distribution, $2D_a^{obs}$, because the probability of observing the largest RDC is proportional to $\sin\theta$ and θ tends to zero. The position, in a distribution of RDCs (see Fig. 7) occuring with the highest frequency is located at $D_a^{obs}(-1 + 3R^{obs}/2)$. In many cases, however, this maximum value is also not well defined due to the limited number of experimental RDCs. Quantitatively, this limitation can be expressed by the width of the histogram bin size, W, $(W = 2(IQR)N^{-1/3})$ [39], where N is the total number

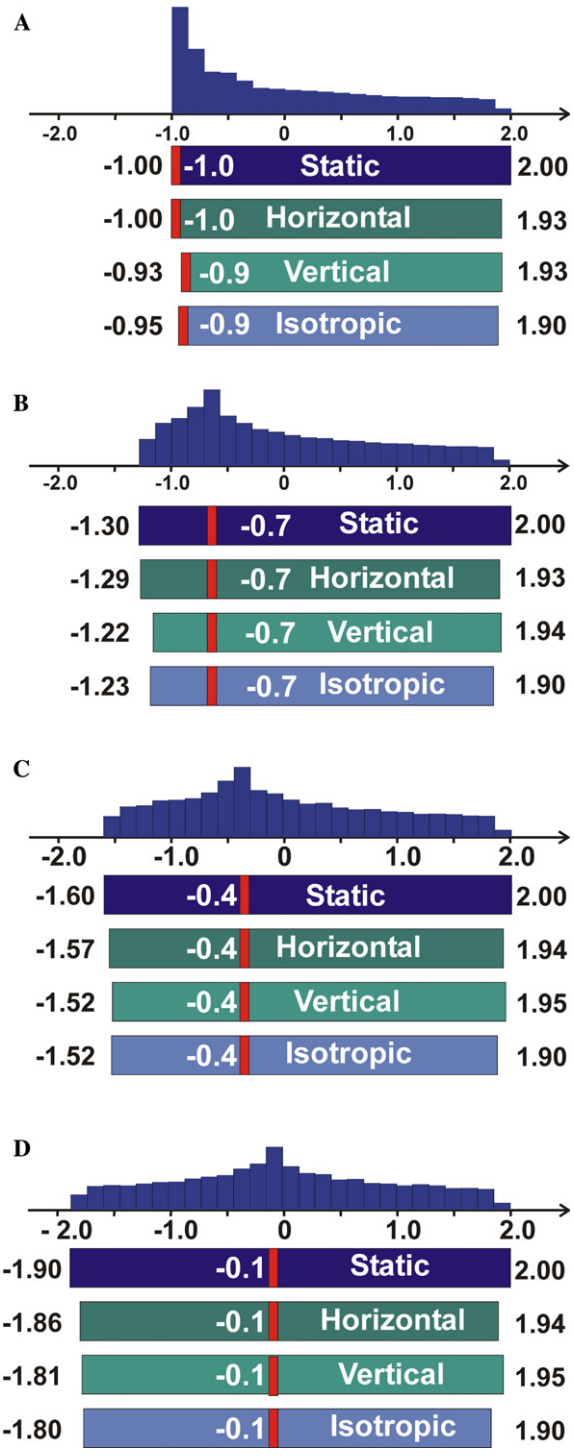

Fig. 7. Histograms of the distributions calculated for the static, isotropic, horizontal, and vertical motional models, using $\beta_{\max} = 15°$, $D_a = 1$ Hz, and (A) $R = 0.0$, (B) 0.2, (C) 0.4, and (D) 0.6. For each dynamic model the distribution of RDCs was formed from 6316 vectors. The width of the bin for each histogram is 0.15 Hz (illustrating the level of precision when 6316 different orientations are used). The numbers on the left and right hand sides are the lower $(-D_a^{\text{obs}}(1 + 3R^{\text{obs}}/2))$ and upper $(2D_a^{\text{obs}})$ bounds of each distribution respectively. The red bar and number beneath each histogram represent the position and magnitude (Hz) of the RDC occurring with the greatest probability, for which, in the majority of cases, no change can be detected.

of RDCs and *IQR* is the interquartile range (the 75th percentile minus the 25th percentile). The *IQR* corresponds to the central 50% of the data, and thus is not affected by outliers [39]. For example, for a simulated uniform distribution of 6316 RDCs with $D_a = 1$ Hz and $R = 0.3$ having a total span of 3.45 Hz, it is found that 1579 RDCs (25% of the total) are less than -0.72 Hz (which is the 25th percentile), 4737 RDCs (75% of the total) are less than $+0.71$ Hz (which is the 75th percentile) and the *IQR* value, in this case, is defined by $IQR = 0.71 - (-0.72) = 1.43$ Hz. Thus, in the case of 6316 RDCs, the optimum histogram bin size is 0.15 Hz, which is relatively large considering the number of RDCs used in this simulation, and corresponds to a total of 23 bins. In the case of a total of 500 RDCs, the optimum histogram has a bin width $W = 0.36$ Hz with a total of 10 bins; for a total of 100 RDCs the histogram will be made up of 6 bins having a width $W = 0.62$ Hz. Consequently, the maximum value of the distribution is not well defined, especially when the number of RDCs is $\ll$6316, which will, typically, be the case in an experimental situation even allowing for a number of different sets of internuclear vectors.

B.2. Models of local motion and the effect on a distribution of RDCs

To compare the influence of the different types of internal motion upon D_a^{obs} and R^{obs}, four distributions of RDCs were simulated using Eqs. (1), (7), (14), and (15), assuming $\beta_{\max} = 15°$, and $D_a = 1$ Hz. A uniform distribution of RDCs was formed using 6316 unit vectors and for each motional model, four different values, (0, 0.2, 0.4, and 0.6), were employed for R. Histograms of the dipolar couplings are shown in Fig. 7. In order to assess the differential changes to the distributions from the different types of local internal motion, the changes to the upper and lower bounds and to the maximum of each distribution were monitored. The effect of experimental noise on the distribution of RDCs has been treated in [40]. An additional distribution made of 12,632 RDCs, which is not represented in Fig. 7, was also generated by superimposing the distributions from the horizontal and vertical models. This corresponds to the situation where both types of unidimensional motions occur simultaneously, for distinct internuclear vectors; this situation is referred to as "Mixed" in the first table of Appendix B.2. The parameters D_a^{obs} and R^{obs} inferred from the upper and lower bounds of each distribution, were calculated and the results are shown in the first table of Appendix B.2. The results for isotropic internal motion are quite simple: the new distribution influenced by motion can be obtained by a homotethy from the distribution of the static model. For each value of R, the RDC are proportional to $D_a^{\text{obs}} = D_a S_{\text{iso}}$ and R^{obs} is equal to R (first table of Appendix B.2). If the motion is

isotropic, and S_{iso} is the same for all pairs of nuclei, the effect of the motion is to scale down the coefficient D_a, allowing only the determination of $D_a^{obs} = D_a S_{iso}$. However, if S_{iso} is *not* the same for all pairs of nuclei, this general statement no longer applies. Horizontal internal motion is estimated to have only a relatively small effect on the lower bound of the distribution with a maximum effect of +0.04 Hz (~2.1%), representing only a relatively small difference compared to the static model, Fig. 5D. The maximum impact on the upper bound is −0.07 Hz, occuring when R is small and compared to the static model reduces D_a^{obs} by ~3.5%. R^{obs} is calculated to be systematically larger than R, by +0.024 when $R = 0$ and by +0.011 when $R = 0.6$, and the change is most significant when R is small (first table of Appendix B.2). For vertical internal motion, the maximum effect on the lower and upper bounds, compared to the static model, is +0.09 and −0.07 Hz, respectively, and in each case, the value for D_a^{obs} is smaller than D_a by ~3%. R^{obs} is reduced compared to R and when $R = 0.2$ the difference is calculated to be about 14%. The changes to R^{obs} are seen to be quite different between the vertical and horizontal motional models, where R^{obs} is respectively either larger or smaller over the complete range of R (see first table of Appendix B.2). If the distributions corresponding to unidimensional horizontal and vertical motions are superimposed (first table of Appendix B.2, "Mixed"), assuming each local motion occurs simultaneously but on separate dipolar vectors, the value for D_a^{obs} is found to be similar to vertical motion over the whole range of R. However, R^{obs} is systematically larger than R, thus following to some extent the behaviour of horizontal unidimensional motion; the changes are more significant at low R values. In the discussion above, we have assumed that each vector undergoes identical motional amplitude of 15°, hence additional effects might be expected if there is a spread in the amplitudes of the local motion. These effects are discussed in the following subsection. To gain quantitative insight into the amplitude of local internal motion, Lipari and Szabo [12] introduced the order parameter S^2_{LS}. S^2_{LS} is typically determined from a series of heteronuclear relaxation datasets and Tjandra et al. [15] measured S^2_{LS} for each NH internuclear vector in ubiquitin. A histogram of the $(S^2_{LS})^{1/2}$ values is shown in Fig. 8. Assuming each order parameter is associated with isotropic internal motion in a cone, the resulting distribution of cone semi-angles is displayed in Fig. 8B. The median cone angle β_{max}

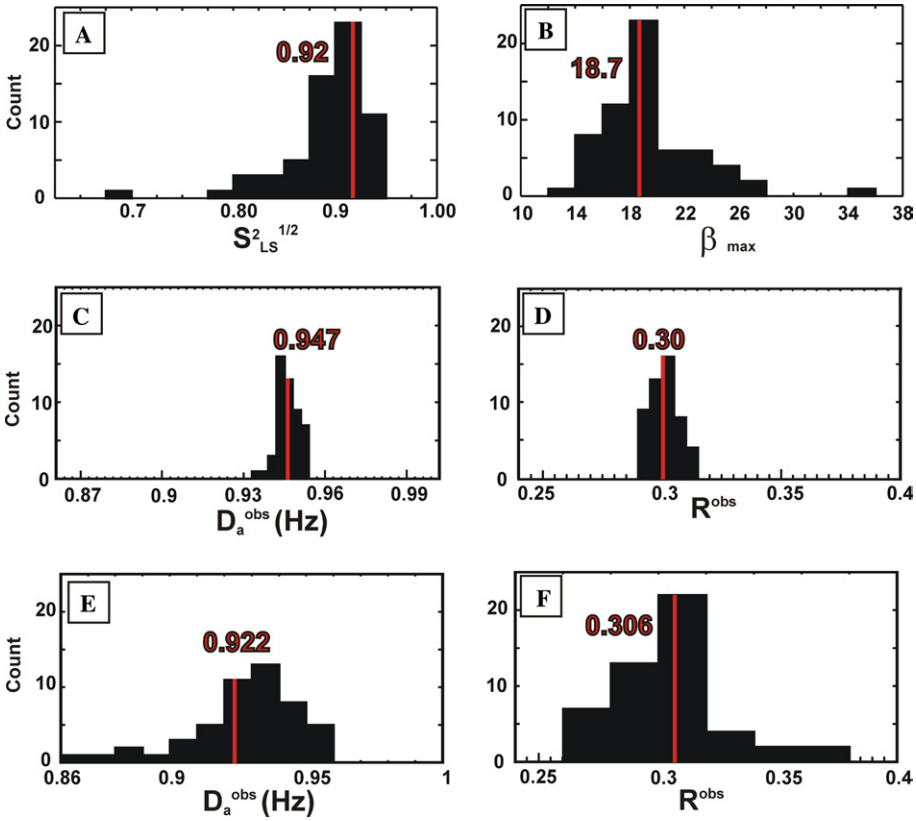

Fig. 8. Histograms for (A) $(S^2_{LS})^{1/2}$ for all of the NH vectors in ubiquitin [15], (B) the cone semi-angle β_{max}, assuming isotropic internal motion. Figures for D_a^{obs} (C) and R^{obs} (D). The histograms were formed from 50 separate distributions composed of 6316 vectors using $D_a = 1$ Hz, $R = 0.3$. (E) D_a^{obs} and (F) R^{obs} were calculated from 50 separate distributions of RDC, with each composed of only 120 vectors, using $D_a = 1$ Hz, $R = 0.3$. For the histograms in (C–F), each individual RDC was multiplied by a randomly chosen $(S^2_{LS})^{1/2}$ value from the histogram of (A). For each histogram, the median values of the distributions is shown located by an orange line.

is 18.7° (indicated in orange) and corresponds to a value for S_{iso} of 0.92. In the following, we assume that to evaluate the effect of motion upon a uniform distribution of RDCs, using Eq. (7), in the case that each RDC is associated with a different value for S_{iso}, this distribution of order parameters is suitable for selecting individual $S_{iso} = (S^2_{LS})^{1/2}$ values. Each RDC value in a uniform distribution of 6316 dipolar vectors, formed using $D_a = 1$ Hz and $R = 0.3$, was multiplied by a randomly chosen value from the distribution of $(S^2_{LS})^{1/2}$ values. The process was repeated 50 times and the values for D_a^{obs} and R^{obs} obtained in each case are shown as histograms in Figs. 8C and D, using a bin width of 0.003 and 0.005 (the optimum value with $N = 50$ and IQR = 0.005 and 0.009, respectively). The median value for R^{obs} of 0.300, Fig. 8D, is not significantly changed from its initial value R, but, the median value for the quantity $D_a^{obs} = 0.95$, changes by about 3%, which is slightly greater than $D_a(S^2_{LS})^{1/2}_{med} = 0.92$. Hence, when each RDC has a different S_{iso} value, fast internal isotropic local motions can cause D_a^{obs} to change slightly while the rhombicity ratio, R^{obs}, is essentially equal to R. The spread in the distributions of D_a^{obs} and R^{obs} characterized by their standard deviation is rather small, corresponding respectively to 0.5% and 2% of the median values. The value for the quantity D_a^{obs} of 0.95 corresponds to D_a multiplied by the maximum expected from the distribution of $(S^2_{LS})^{1/2}$ values employed here. This value most likely arises because of the large number of RDCs included in the simulations and, therefore, the maximum value for $(S^2_{LS})^{1/2}$ has a high probability of being used for orientations corresponding to the extrema in the distribution of RDCs. A further four distributions with a smaller number of vectors (1105, 562, 302, and 120 vectors) were also used to calculate D_a^{obs} and R^{obs} and the results are shown in the second table of Appendix B.2. For $N = 120$, the histograms for D_a^{obs} and R^{obs} are shown in Figs. 8E and F. For 120 vectors, the median value for D_a^{obs}, 0.93, is closer to the median value for $(S^2_{LS})^{1/2}$ and the median for R^{obs} of 0.306 is very close to the true value for $R = 0.3$, and is only overestimated by ~2%. For $N = 120$, the standard deviations of the values for D_a^{obs} and R^{obs} are 2.2% and 8%, respectively of the median values respectively, reducing to 0.5% and 2% if 6316 vectors are used, second table of Appendix B.2. With a distribution of 120 vectors, the average value of $(S^2_{LS})^{1/2}$ is the dominant factor in determining D_a^{obs} and R^{obs} with large standard deviations. With 6316 vectors, the maximum value for $(S^2_{LS})^{1/2}$ is the dominant factor with the standard deviations for D_a^{obs} and R^{obs} now small. This phenomenon is most likely explained by the simultaneous presence of two factors, namely the spread in $(S^2_{LS})^{1/2}$ values and the density of the orientational sampling (even if the positions corresponding to the maxima are sampled). A sharp fall in the standard deviations for D_a^{obs} and R^{obs} (by factors of 6 and 2, respectively) is observed between 120 and 1105 vectors (second table of Appendix B.2) whereas only minor changes are found when a further 5000 vectors are added to the distribution. The values of D_a^{obs} and R^{obs} are not affected at all by the presence of one residue featuring a small $(S^2_{LS})^{1/2}$ value (lower than 0.7, Fig. 8), because in each case, the density of the sampling of dipolar vectors near the orientations corresponding to the RDC maxima is sufficient to balance the effect of the lowest $(S^2_{LS})^{1/2}$ factors. When 120 vectors are used, the lowest D_a^{obs} is equal to 0.86, which is much higher than 0.7.

The values of D_a^{obs} and R^{obs} calculated form the lower $(-D_a^{obs}(1 + 3R^{obs}/2))$ and upper $(2D_a^{obs})$ bounds of the distribution of RDC shown in Fig. 7

	$R = 0.0$	$R = 0.2$	$R = 0.4$	$R = 0.6$
D_a^{obs}				
Static	1.000	1.000	1.000	1.000
Horizontal	0.965	0.965	0.970	0.970
Vertical	0.965	0.970	0.975	0.975
Mixed	0.965	0.970	0.975	0.975
Isotropic	0.950	0.950	0.950	0.950
R^{obs}				
Static	0.000	0.200	0.400	0.600
Horizontal	0.024	0.225	0.412	0.611
Vertical	−0.024	0.172	0.372	0.571
Mixed	0.024	0.220	0.407	0.605
Isotropic	0.000	0.200	0.400	0.600

Table of the median values and standard deviations for D_a^{obs} and R^{obs} back-calculated from 5 sets of 50 distributions of RDC using N dipolar vectors ($N = 120$, 302, 562, 1105, and 6316)

N	D_a^{obs}	SD	R^{obs}	SD
120	0.922	0.034	0.306	0.024
302	0.933	0.012	0.302	0.015
562	0.934	0.01	0.301	0.015
1105	0.934	0.006	0.299	0.012
6316	0.947	0.004	0.3	0.006

An isotropic motional model has been used, with $D_a = 1$ Hz and $R = 0.3$ where each RDC value was multiplied by a randomly chosen value from the distribution of $(S^2_{LS})^{1/2}$ values (obtained from the relaxation experiments made on ubiquitin, Figs. 8A and B).

B.3. Conclusion

The maximum influence of the particular types of motions considered here upon D_a^{obs}, the value of D_a determined from the motionally averaged distribution of RDC values, is less than 5% when $\beta_{max} \leqslant 20°$. However, the effect of motion upon R is found to be quite

model dependent and compared to the static and isotropic models the influence of horizontal or vertical motions upon the value determined from the distribution of RDCs, R^{obs}, can be 14%.

Appendix C. The effect of motional amplitude and motional anisotropy upon the determination of θ_{av} and ϕ_{av} from an individual RDC

The equivalent angular horizontal and vertical displacements, θ_{hor} and θ_{ver}, needed to account for the effect of horizontal, vertical, and isotropic dynamics upon the RDC when using a static model have been calculated for different values of β_{max} ($\beta_{max} \leqslant 30°$) employing a random distribution of 562 internuclear vectors. The results are shown in Figs. 9A, B, and C, respectively. For each dynamic model the minimum and maximum, the average value and the standard deviation for the calculated θ_{hor} and θ_{ver} angles are shown. The angles were computed in the following manner. For each internuclear vector in the random ensemble, oriented by θ_{av} and ϕ_{av}, the left hand side (LHS) of Eqs. (C.1), (C.2), and (C.3) were computed using Eq. (15), (14), and (7) with $D_a = 1$ Hz, $R = 0.3$ and variable β_{max} values. θ_{hor} and θ_{ver} were calculated from the right-hand side of the following relationships.

$$(RDC^{exp} + \Delta^{RDC}_{dyn})_{hor} = RDC(\mathbf{v}''(\theta_{hor})). \tag{C.1}$$

The definition of the vector $\mathbf{v}''(\theta_{hor})$ is given by Eq. (6).

$$(RDC^{exp} + \Delta^{RDC}_{dyn})_{ver} = D_a\left[(3\cos^2(\theta_{av}+\theta_{ver})-1) + \frac{3}{2}R\sin^2(\theta_{av}+\theta_{ver})\cos 2\phi_{av}\right], \tag{C.2}$$

$$(S_{iso}RDC_{exp})_{iso} = D_a\left[(3\cos^2(\theta_{av}+\theta_{ver})-1) + \frac{3}{2}R\sin^2(\theta_{av}+\theta_{ver})\cos 2\phi_{av}\right]. \tag{C.3}$$

In the case of isotropic motion the equivalent equation containing θ_{hor} instead of θ_{ver}, i.e., $(S_{iso}RDC_{exp})_{iso} = RDC(\mathbf{v}''(\theta_{hor}))$, does not always have a solution. For example, when $R = 0$ and $\theta_{av} = 90°$, the static RDC is $-D_a$ and a horizontal angular displacement leaves the vector in the equatorial plane where the RDC is unaffected and in this case no value for θ_{hor} can satisfy the LHS of this equation. The average value for θ_{ver} from either vertical or isotropic motion is very small, whereas, for horizontal motion there is a slightly larger average value for θ_{hor} and its standard deviation is also larger reaching ~5° when $\beta_{max} = 20°$. The standard deviations for θ_{ver} are lower for both types of

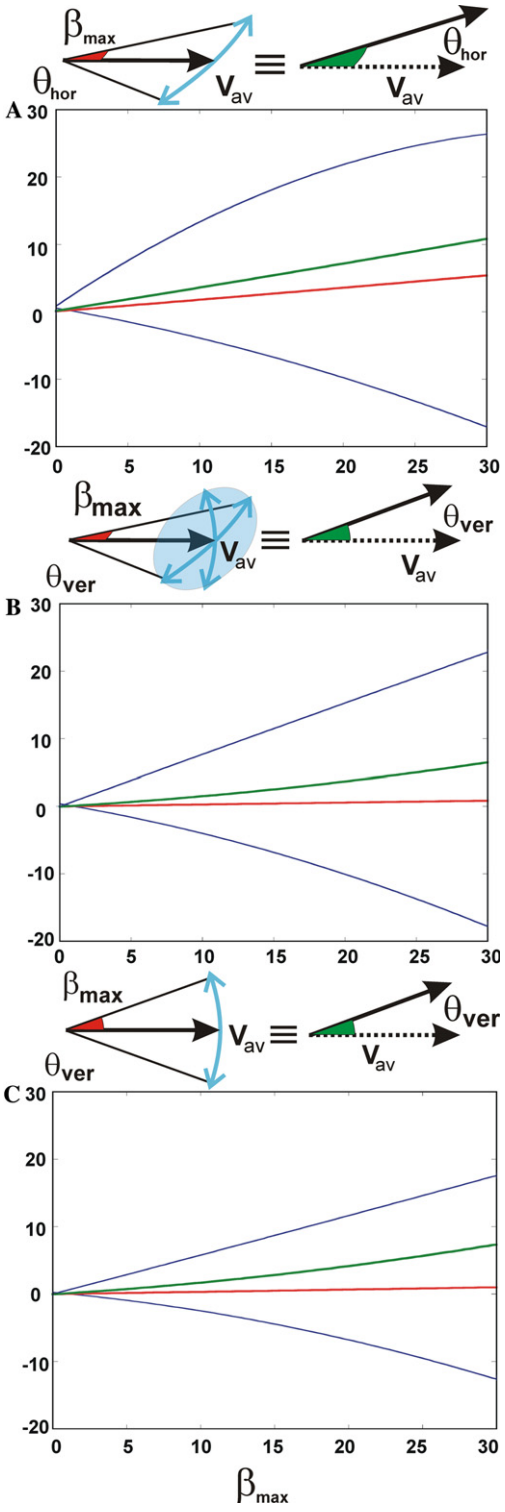

Fig. 9. Values for the maximum and minimum (blue), the average (red), and the standard deviation (green) for the angular corrections θ_{hor} and θ_{ver} are shown as a function of β_{max}. For each vector (θ_{av}, ϕ_{av}) in the distribution RDC^{exp} has been generated using a static model, Eq. (1), with $D_a = 1$ Hz and $R = 0.3$ and Δ^{RDC}_{dyn} was computed using either Eq. (16) or Eq. (15) or Eq. (7). The angular corrections θ_{hor} and θ_{ver} were calculated from Eqs. (C.1), (C.2), and (C.3).

motion and reach ~3° when $\beta_{max} = 20°$. Whatever the form of the continuous internal motion the average RDC, formed from the ensemble of allowed conformations for each internuclear vector, has a similar orientation ($\theta_{back}, \phi_{back}$) to at least one vector in the ensemble (which is a consequence of the mean value theorem) but this vector is not necessarily the vector in the average angular orientation (θ_{av}, ϕ_{av}). Consequently the back calculated orientation ($\theta_{back}, \phi_{back}$) using the averaged RDC lies within the ensemble of conformations but may be tilted from the average angular orientation (θ_{av}, ϕ_{av}).

We note that a fraction of the effect of motional averaging can be captured by the alignment tensor (D_a^{obs} value, cf. Appendix B), however, this would not absorb any additional motion observed for a specific internuclear vector. For example, if all the vectors but one experience isotropic motional averaging with the same amplitude (the RDC is scaled down by S_{iso}), the effect of motion for these vectors would be captured by $D_a^{obs} = S_{iso} D_a$. If one of them undergoes the same isotropic motion superimposed with uni-dimensional motion, its *RDC* will be given by Eq. (16). Hence, if this isotropic motion is undetected, the effect of the unidimensional motion remains for this particular vector, and the approach used above allow us to link the effect of an additional motional averaging process (Δ_{dyn}^{RDC}) to the angular precision of the model structure concerning this particular vector.

References

[1] L.C. Snyder, Analysis of nuclear magnetic resonance spectra of molecules in liquid-crystal solvents, J. Chem. Phys. 43 (1965) 4041–4050.

[2] R.E.J. Sears, E.L. Hahn, Upper limits to electric-field-induced nuclear magnetic dipole–dipole couplings in polar liquids, J. Chem. Phys. 45 (1966) 2753–2769.

[3] J.D. Macomber, N.S. Ham, J.S. Waugh, Upper limit to the electric-field effect on the NMR spectrum of nitromethane, J. Chem. Phys. 46 (1967) 2855–2856.

[4] A.D. Buckingham, K.A. McLaughlan, High resolution nuclear magnetic resonance in partially oriented molecules, Prog. NMR. Spectrosc. 2 (1967) 63–109.

[5] J.W. Emsley, J.W. Lindon, NMR Spectroscopy Using Liquid Crystal Solvents, Pergamon Press, Oxford, 1975.

[6] J. Lohman, C. MacLean, Magnetic field induced alignment effects in ^{2}H NMR spectra, Chem. Phys. Lett. 58 (1978) 483–486.

[7] J.R. Tolman, J.M. Flanagan, M.A. Kennedy, J.H. Prestegard, Nuclear magnetic dipole interactions in field-oriented proteins: information for structure determination in solution, Proc. Natl. Acad. Sci. USA 92 (1995) 9279–9283.

[8] N. Tjandra, A. Bax, Direct measurement of distances and angles in biomolecules by NMR in a dilute liquid crystalline medium, Science 278 (1997) 1111–1114.

[9] M.R. Hansen, L. Mueller, A. Pardi, Tunable alignment of macromolecules by filamentous phage yields dipolar coupling interactions, Nat. Struct. Biol. 5 (1998) 1065–1074.

[10] R. Tycko, F.J. Blanco, Y. Ishii, Alignment of biopolymers in strained gels: a new way to create detectable dipole–dipole couplings in high-resolution biomolecular NMR, J. Am. Chem. Soc. 122 (2000) 9340–9341.

[11] N. Tjandra, J.G. Omichinski, A.M. Gronenborn, G.M. Clore, A. Bax, Use of dipolar ^{1}H–^{15}N and ^{1}H–^{13}C couplings in the structure determination of magnetically oriented macromolecules in solution, Nat. Struct. Biol. 4 (1997) 732–738.

[12] G. Lipari, A. Szabo, Model-free approach to the interpretation of nuclear magnetic resonance relaxation in macromolecules. 1. Theory and range of validity, J. Am. Chem. Soc. 104 (1982) 4546–4559.

[13] J.R. Tolman, H.M. Al-Hashimi, L.E. Kay, J.H. Prestegard, Structural and dynamic analysis of residual dipolar coupling data for proteins, J. Am. Chem. Soc. 123 (2001) 1416–1424.

[14] W. Peti, J. Meiler, R. Brüschweiler, C. Griesinger, Model-free analysis of protein backbone motion from residual dipolar couplings, J. Am. Chem. Soc. 124 (2002) 5822–5833.

[15] N. Tjandra, S.E. Feller, R.W. Pastor, A. Bax, Rotational diffusion anisotropy of human ubiquitin from ^{15}N NMR relaxation, J. Am. Chem. Soc. 117 (1995) 12562–12566.

[16] G.M. Clore, C.D. Schwieters, How much backbone motion in ubiquitin is required to account for dipolar coupling data measured in multiple alignment media as assessed by independent cross-validation?, J. Am. Chem. Soc. 126 (2004) 2923–2938.

[17] D.M. Korzhnev, M. Billeter, A.S. Arseniev, V.Y. Orekhov, NMR studies of Brownian tumbling and internal motions in proteins, Prog. Nucl. Magn. Reson. Spectrosc. 38 (2001) 197–266.

[18] K. Yamasaki, M. Saito, M. Oobatake, S. Kanaya, Characterization of the internal motions of Escherichia coli ribonuclease HI by a combination of ^{15}N-NMR relaxation analysis and molecular dynamics simulation: examination of dynamic models, Biochemistry 34 (1995) 6587–6601.

[19] D. Fushman, O. Ohlenschlager, H. Rüterjans, Determination of the backbone mobility of ribonuclease T1 and its 2′GMP complex using molecular dynamics simulations and NMR relaxation data, J. Biomol. Struct. Dyn. 11 (1994) 1377–1402.

[20] K.V. Pervushin, V.Y. Orekhov, D.M. Korzhnev, A.S. Arseniev, Manifestation of intramolecular motions on picosecond and nanosecond time scales in H-1–N-15 NMR relaxation—analysis of dynamic-models of one-helical and 2-helical subunits of bacterioopsin, J. Biomol. NMR 5 (1995) 383–396.

[21] M.H. Levitt, Spin dynamics, Basics of Nuclear Magnetic Resonance, Wiley, Chichester, England, 2001.

[22] T. Bremi, R. Brüschweiler, Locally anisotropic internal polypeptide backbone dynamics by NMR relaxation, J. Am. Chem. Soc. 119 (1997) 6672–6673.

[23] S.F. Lienin, T. Bremi, B. Brutscher, R. Brüschweiler, R.R. Ernst, Anisotropic intramolecular backbone dynamics of ubiquitin characterized by NMR relaxation and MD computer simulation, J. Am. Chem. Soc. 120 (1998) 9870–9879.

[24] J. Meiler, J.J. Prompers, W. Peti, C. Griesinger, R. Brüschweiler, Model-free approach to the dynamic interpretation of residual dipolar couplings in globular proteins, J. Am. Chem. Soc. 123 (2001) 6098–6107.

[25] J. Meiler, W. Peti, C. Griesinger, Dipolar couplings in multiple alignments suggest alpha-helical motion in ubiquitin, J. Am. Chem. Soc. 125 (2003) 8072–8073.

[26] P. Bernardo, M. Blackledge, Anisotropic small amplitude peptide plane dynamics in proteins from residual dipolar couplings, J. Am. Chem. Soc. 126 (2004) 4907–4920.

[27] P. Bernardo, M. Blackledge, Local dynamic amplitudes on the protein backbone from dipolar couplings: toward the elucidation of slower motions in biomolecules, J. Am. Chem. Soc. 126 (2004) 7760–7761.

[28] N. Tjandra, S. Grzesiek, A. Bax, Magnetic field dependence of nitrogen-proton J splittings in ^{15}N-enriched human ubiquitin resulting from relaxation interference and residual dipolar coupling, J. Am. Chem. Soc. 118 (1996) 6264–6272.

[29] The maximum difference between these two models is equal to $\Delta_{RDC}^{dyn}(\text{vertical}) - \Delta_{RDC}^{dyn}(\text{horizontal}) = \beta_{max}^2 D_a(\sin^2\theta_{av} + R(1+$

$\cos^2\theta_{av})\cos 2\phi_{av}/2)$. This function takes a value between $-\beta^2_{max}D_aR$ and $\beta^2_{max}D_a(1+R/2)$, which corresponds to approximately -0.02 Hz (-1% of the maximum RDC) and 0.08 Hz ($+4\%$ of the maximum RDC) for $D_a = 1$ Hz, $R = 0.3$, $\beta_{max} = 15°$.

[30] T.S. Ulmer, B.E. Ramirez, F. Delaglio, A. Bax, Evaluation of backbone proton positions and dynamics in a small protein by liquid crystal NMR spectroscopy, J. Am. Chem. Soc. 125 (2003) 9179–9191.

[31] P. Hodgkinson, P.J. Hore, in: W.S. Warren (Ed.), Advances in Magnetic and Optical Resonance, Academic Press, San Diego, 1997, p. 187.

[32] P. Diehl, Structure of Rigid Molecules dissolved in Liquid Crystalline Solvents, Encyclopedy of Nuclear Magnetic Resonance, Wiley, New York, 1996, pp. 4591–4602.

[33] M. Ottiger, A. Bax, Determination of relative N–HN, N–C′, C^α–C′, and C^α–H^α effective bond lengths in a protein by NMR in a dilute liquid crystalline phase, J. Am. Chem. Soc. 120 (1998) 12334–12341.

[34] M. Ottiger, A. Bax, How tetrahedral are methyl groups in proteins? A liquid crystal NMR study, J. Am. Chem. Soc. 121 (1999) 4690–4695.

[35] D. Yang, J.R. Tolman, N.K. Goto, L. Kay, An HNCO-based pulse scheme for the measurement of $^{13}C^\alpha$–$^1H^\alpha$ one-bond dipolar couplings in 15N, 13C labeled proteins, J. Biomol. NMR 12 (1998) 325.

[36] C. Jelsch, M. Teeter, V. Lamzin, V. Pichon-Lesme, B. Blessing, C. Lecomte, Accurate protein crystallography at ultra-high resolution: valence electron distribution in crambin, Proc. Natl. Acad. Sci. USA 97 (2000) 3171–3176.

[37] M. Zweckstetter, A. Bax, Evaluation of uncertainty in alignment tensors obtained from dipolar couplings, J. Biomol. NMR 23 (2002) 127–137.

[38] D. Fushman, R. Ghose, D. Cowburn, The effect of finite sampling on the determination of orientational properties: a theoretical treatment with application to interatomic vectors in proteins, J. Am. Chem. Soc. 122 (2000) 10640–10649.

[39] A. Izenman, Recent developments in nonparametric density estimation, J. Am. Stat. Assoc. 86 (1991) 205–224.

[40] G.M. Clore, A.M. Gronenborn, A. Bax, A robust method for determining the magnitude of the fully asymmetric alignment tensor of oriented macromolecules in the absence of structural information, J. Magn. Reson. 133 (1998) 216–221.